

Synthesis and Applications of Two-Dimensional Hexagonal Boron Nitride in Electronics Manufacturing

Jie Bao,^{1,2} Kjell Jeppson,^{1,3} Michael Edwards,³ Yifeng Fu,^{3,4} Lilei Ye,⁴ Xiuzhen Lu,¹ and Johan Liu^{1,3,*}

¹SMIT Center, School of Automation and Mechanical Engineering and Key State Laboratory of New Displays and System Applications, Shanghai University, Shanghai, 200072, China

²School of Mechanical and Electrical Engineering, Huangshan University, Huangshan, 245041, China

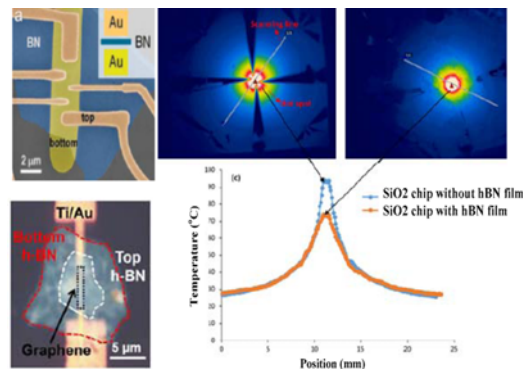
³Department of Microtechnology and Nanoscience, Chalmers University of Technology,
41296 Gothenburg, Sweden

⁴SHT Smart High Tech AB. Aschebergsgatan 46, 41133, Gothenburg, Sweden

(received date: 21 July 2015 / accepted date: 8 October 2015 / published date: 10 January 2016)

In similarity to graphene, two-dimensional (2D) hexagonal boron nitride (hBN) has some remarkable properties, such as mechanical robustness and high thermal conductivity. In addition, hBN has superb chemical stability and it is electrically insulating. 2D hBN has been considered a promising material for many applications in electronics, including 2D hBN based substrates, gate dielectrics for graphene transistors and interconnects, and electronic packaging insulators. This paper reviews the synthesis, transfer and fabrication of 2D hBN films, hBN based composites and hBN-based van der Waals heterostructures. In particular, this review focuses on applications in manufacturing electronic devices where the insulating and thermal properties of hBN can potentially be exploited. 2D hBN and related composite systems are emerging as new and industrially important materials, which could address many challenges in future complex electronics devices and systems.

Keywords: two-dimensional hexagonal boron nitride, electronics manufacturing, van der waals heterostructures



1. INTRODUCTION

The Nobel prize awarded to Andre Geim and Kostya Novosolov in 2010 boosted the research on graphene, has now become a hot research topic and thousands of papers published every year.^[1] Recently, research focus has shifted from studies of the graphene material itself to its application in a diverse range of fields.^[2] Among the two-dimensional materials, graphene exhibits the best mechanical strength, as well as the highest electrical and thermal conductivities.^[3] However, graphene is a conductor which limits its application

in some fields such as memory, capacitors, and gate dielectrics.^[4] Recently, an alternative two-dimensional electrically insulating material, 2D hBN or white graphene as it is also known, has attracted a great deal of attention.^[1,6]

One very important property of bulk hBN crystals is that they are exceptional substrates for graphene growth, allowing a tenfold increase in the electronic quality of graphene.^[6] Two-dimensional hBN consists of a lattice structure similar to that of graphene. Its unique properties make 2D hBN a promising nanomaterial for applications in a variety of fields. These applications include its use in devices operating at high temperatures in oxidative environments,^[7] and in insulating composites due to its high elastic moduli (0.5 - 0.6 TPa)^[8] and thermal conductivity (390 W/m·K).^[9] Finally,

*Corresponding author: johan.liu@chalmers.se
©KIM and Springer

its use as electrically insulating substrates that are perfectly lattice matched to graphene^[10,11] should be noted. In this paper, the progress made in synthesis, transfer, and application of 2D hBN and hBN/graphene heterostructures in electronics manufacturing will be reviewed. In particular, this paper will concentrate mechanical and liquid-phase exfoliation, as well as chemical vapor deposition (CVD) synthesis methods. The key post processing steps for a hBN film, depending on application, are the transfer of the film and the fabrication hBN-based Van der Waals heterostructures with other 2D materials, such as graphene. This paper will then describe two key applications for hBN in electronics, for electrical insulation in advanced packaging and as a heat spreader for power devices and chips. The paper shall conclude by giving a brief perspective on hBN-based technologies and their potential for industry.

2. SYNTHESIS OF TWO-DIMENSIONAL HEXAGONAL BORON NITRIDE

The physicochemical properties of 2D hBN, to a great extent, depend on how it is synthesized, meaning that suitable synthesis methods should be selected according to the application. The three most commonly used methods to synthesize 2D hBN are: mechanical exfoliation, liquid-phase exfoliation and chemical vapor deposition (CVD). On the one hand, mechanical exfoliation can result in perfect crystalline hBN structures,^[12] yet the yield is very low.

Liquid-phase exfoliation is an efficient method for producing large quantities of layered hBN,^[13-17] however, the number of layers and their lateral size are difficult to control in contrast with mechanical exfoliation. On the other hand, the dry CVD method has the promised benefit of fine control over the number of layers and the crystalline structures as shown

in the literature.^[18,19] In the following sub-sections, these three major synthesis methods and some other specifically developed methods will be reviewed.

2.1 Mechanical exfoliation

Mechanical cleavage by Scotch tape which was the first method used to fabricate free-standing graphene^[20] has been proven to work also for other layered materials, such as hBN.^[11] The aim of this method is to break the weak van der Waals interaction between layers while leaving the strong sp² bonded in-plane structure intact. Mechanically peeled 2D hBN sheets have fewer defects than those produced by chemical methods. Therefore sheets produced by the exfoliation method are used to explore the intrinsic properties of these 2D materials.^[5] However, mechanical cleavage by Scotch tape has an extremely low yield (<<9%). Li *et al.*^[21] demonstrated that a fully controlled ball milling process can supply a large quantity of high-quality BN nanosheets with little damage to the in-plane crystal structure, as shown in Fig. 1, introducing only a very small amount of point defects or impurities. They chose a planetary mill which controlled balls in rolling actions that only applied shear forces on the milling materials, meaning that it would not destroy crystalline structures, leading to the formation of amorphous or non-equilibrium phases. In addition, their use of large number of small steel balls and a liquid controlling agent also helped to minimize the damage to the in-plane crystal structure.

2.2 Liquid-phase exfoliation

Liquid-phase exfoliation creates dispersions of 2D layered hBN in various solvents or aqueous surfactant solutions with the assistance of sonication.^[5,13-17] Basically, boron nitride micron-powder is scattered into a specific solvent to form a

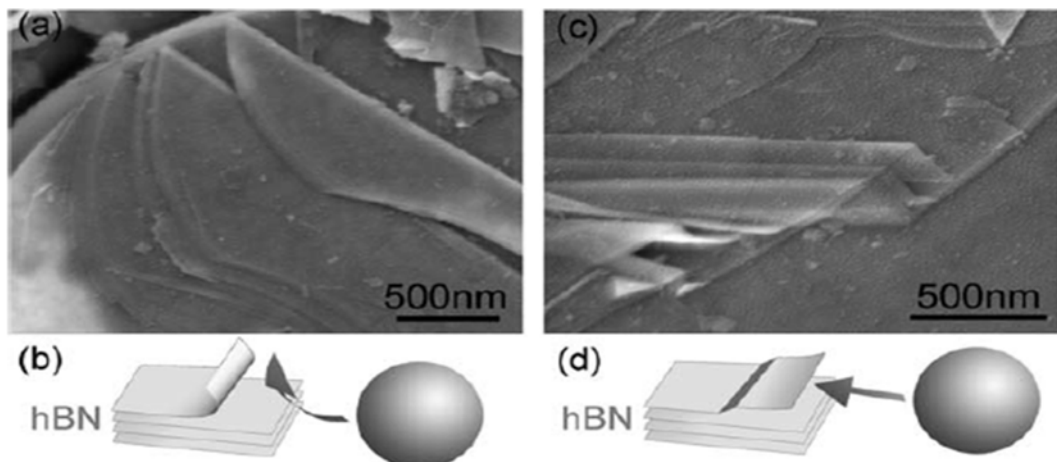


Fig. 1. SEM photos and corresponding diagrams illustrating two observed exfoliating mechanisms under the shear force created by milling balls: (a, b) cleavage from the edge of an hBN particle; (c, d) thin sheets peeled off the top surface of an hBN particle (Taken from ref. 21. Reproduced by permission of Royal Society of Chemistry).

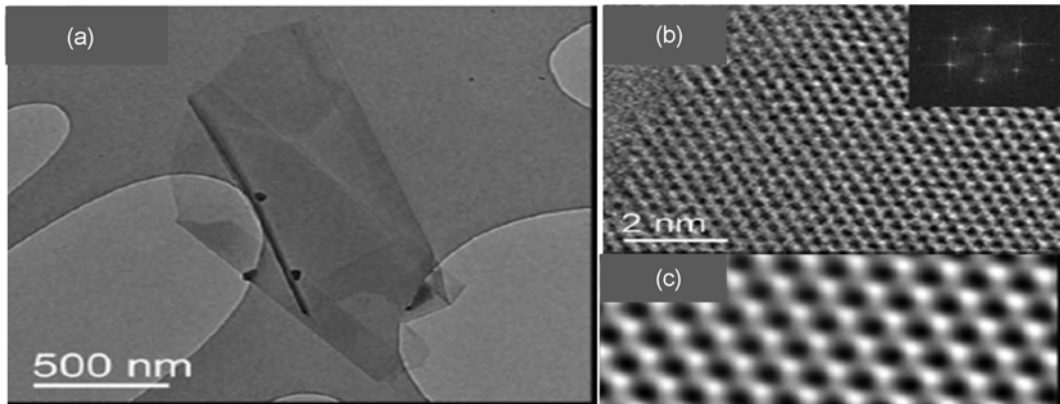


Fig. 2. TEM photos of BN nanosheets; (a) Low-resolution TEM images of BN flakes, (b) high-resolution TEM images of monolayer BN, (c) Butterworth-filtered images of sections of the image in (b) (Taken from ref. 13. Reproduced by permission of American Assn for The Advancement of Science).

low concentration dispersion. Sonication of sufficient intensity breaks the van der Waals forces between the atomic layers of boron nitride. This allows the solvent molecules to seep between the boron nitride layers and expand, assisted by the strong ultrasonication. By using this method the peeling of single hBN layers was achieved, and then it is possible to prepare layered boron nitride, as shown in Fig. 2. This method is quick and easy, and insensitive to ambient conditions, leading to higher yields.

Han *et al.*^[22] showed that the duration of the sonication was an important factor that must be optimized for high yield and low damage to the crystal structure of the final BN sheets. For example, a low intensity of sonication needs a longer duration. Lin *et al.*^[23] showed that the hydrolysis of hBN under sonication participates in the exfoliation, and that this is the main cause of the formation of small sheets of hBN monolayers. Wang *et al.*^[11] used methane sulfonic acid as the solvent, and reported that this kind of protic sulfonic acid was more powerful than commonly used organic solvents such as isopropyl alcohol (IPA) for exfoliating and stabilizing boron nitride nanosheets. Zhou *et al.*^[15] demonstrated a versatile and scalable mixed solvent strategy for liquid exfoliation of hBN in volatile solvents. This was because in their opinion, using nonvolatile solvents makes it difficult to process hBN into devices, due to the difficulties in the removal of solvent and the occurrence of aggregation during the slow solvent evaporation.

Although controlling of the number of layers formed and the lateral size of the flakes is difficult using this method,^[13-16] liquid-phase exfoliation exhibits the ability to produce thin films of inorganic layered compounds with applications in batteries, coatings and lubricants.^[14,15] In addition, the liquid-phase exfoliation method enables the production of a wide range of hybrids with adjustable thermal and electronic conductivity, and attractive thermoelectric properties, as well as composites with enhanced mechanical properties.^[11,17,24-26]

Coleman *et al.*^[13] demonstrated that, by blending individual layers with a suspension of other nanomaterials or polymer solutions, hybrid dispersions or composites can be prepared for a large number of applications.

2.3 Chemical vapor deposition

Chemical vapor deposition (CVD) is probably the most likely method to develop into a technique used for the mass production of 2D layered materials, which is a key requirement for the industrial applications. Bae *et al.*^[18] obtained 30-inch graphene films predominantly composed of monolayers using CVD, and Yamada *et al.*^[19] produced a 294 mm wide graphene film consisting of few layer graphene and nanometer size flakes at a temperature below 400°C. In common with other 2D layered materials, CVD has shown promise in the growth of hBN layers.

The CVD growth process involves four distinct steps: (i) the adsorption of molecules of a precursor gas on the surface with sticking coefficients; (ii) the decomposition of the precursor and formation of mobile surface species; (iii) diffusion of these species; and (iv) nucleation and/or incorporation into the growing film.^[27] Monolayer or few-layer hBN films have been synthesized on single crystal Ru, Rh, Rt, Ni, Pd, Pt, Ag and Cu substrates by using a CVD method with ammonia-borane or borazine as the precursor.^[27-33] As an example, the schematic diagram of LPCVD system used for hBN growth is shown in Fig. 3. The synthesis of large-area ($4 \times 2 \text{ cm}^2$) high quality monolayer hBN with an ultraclean and unbroken surface on Cu foil by using LPCVD is shown in Fig. 4.^[33]

The quality of substrate is one of the most important factors when determining growth behavior such as supercell structure formation and epitaxial growth. Lee *et al.*^[34] studied the influence of the Cu morphology on the high-quality growth of hBN nanosheets. They found that the number of impurity particles on the hBN nanosheets and

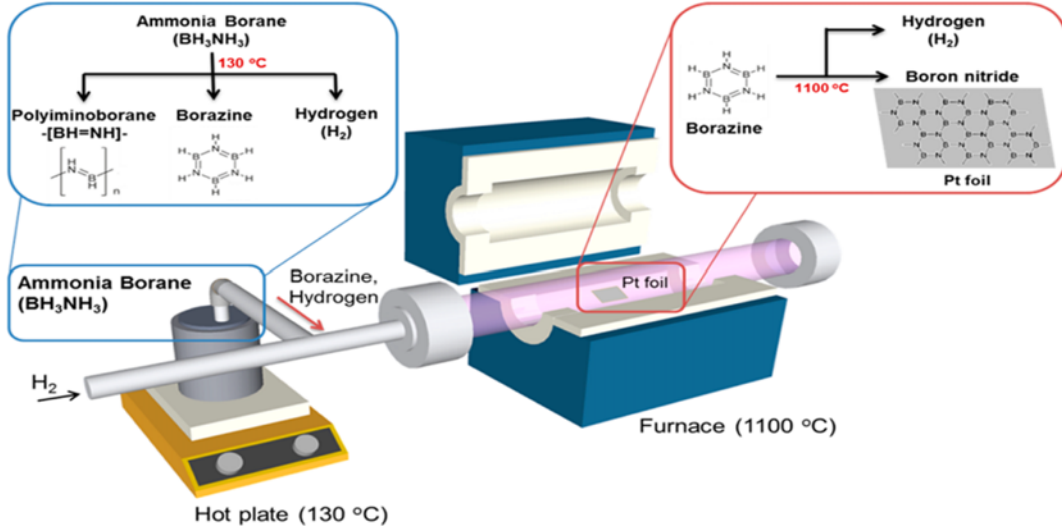


Fig. 3. Schematic diagram of LPCVD system (Taken from ref. 32. Reproduced by permission of American Chemical Society).

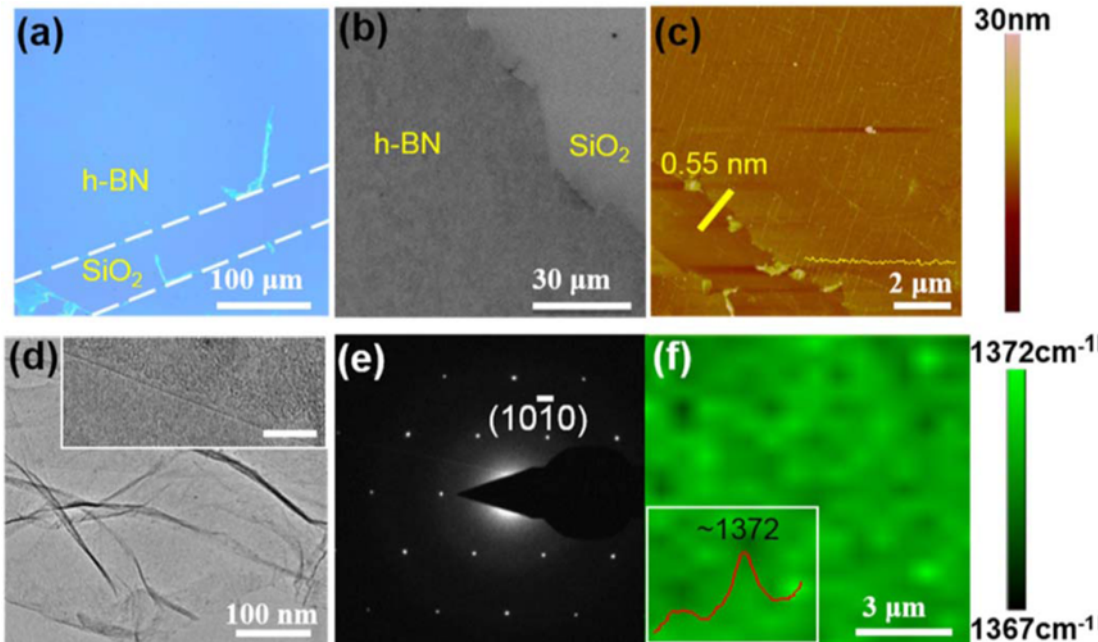


Fig. 4. Images of monolayer hBN on SiO_2/Si substrate observed by. (a) optical microscopy, (b) SEM, (c) AFM, (d) TEM, (e) SAED diffraction pattern of monolayer hBN (f) Raman mapping of monolayer hBN corresponding to the E_{2g} vibration mode; the inset is the Raman spectrum. (Taken from ref. 33. Reproduced by permission of Institute of Physics Publishing).

roughness of the Cu foil were strongly dependent on whether or not the Cu substrate had been subjected to thermal annealing and chemical polishing. Furthermore, the key role of the morphology control of the Cu catalyst is not only resulted in the formation of pure hBN nanosheets with an atomically flat surface, but also an improvement in the crystallinity. Ismach *et al.*,^[35] found that for 30 minutes of growth at 1025°C , BN films on Ni exhibited an ordered layered structure of about 100 layers with a nanocrystalline

termination (n-BN). However, for hBN on sapphire, the growth rate is much lower, with only a few layers appearing to be partially ordered and the rest of the film n-BN.

Recently, Lee *et al.*^[36] presented a promising breakthrough that prevents structural deformations in CVD-grown hBN thin films, by using unintentionally formed nanocrystalline graphene (nc-G) as the catalytic seed layer. By using this method, a wafer-scale ultra-flat hBN thin film was successfully synthesized on a bare sapphire substrate. The authors indicated

Table 1. A list of papers concerned with the effect of growth parameters on the growth behavior of hBN.

Authors	Substrate	Growth parameters	Conclusions
Sutter <i>et al.</i> ^[27]	Ru(0001) single crystals and thin films	borazine pressures	At low borazine pressures, individual hBN domains nucleate sparsely, grow to macroscopic dimensions, and coalesce to form a closed monolayer film.
Song <i>et al.</i> ^[47]	Ni foils	CVD growth time and cooling rates of the substrate	Average thickness of the synthesized hBN films increased with respect to the CVD growth time, and lower cooling rates tended to produce thinner hBN films.
Shi <i>et al.</i> ^[44]	Polycrystalline Ni	Growth temperature	At a moderate temperature (400°C) followed by a 1000°C post-annealing process, a polymerization reaction takes place and forms polyborazylene. This can be further dehydrogenated to form continuous hBN films, without a rough surface morphology or hBN particles.
Orlando <i>et al.</i> ^[48]	Ir(111)	Growth temperature	A single-domain hBN monolayer can be synthesized by a cyclic dose of high-purity borazine onto a metal substrate at room temperature followed by annealing at 1270 K. In contrast, high-temperature borazine deposition ($T = 1070$ K) results in a hBN monolayer formed by domains with an opposite orientation.
Bresnahan <i>et al.</i> ^[49]	Cu foils, a copper enclosure	Partial pressure of precursors	The lower partial pressure of gas-phase BN precursors not only resulted in a decrease in growth rate, but also in an increase in hBN island size, which ultimately led to an enhancement in film crystallinity.

that the sp^3 edges of nc-G play a key role in the formation of hBN with an atomically flat surface on the rough nc-G layer. Tay *et al.*^[37] obtained few- to multi-layer nanocrystalline hBN (NCBN) films directly on both amorphous SiO_2/Si and quartz substrates without any metal catalyst. The as-grown NCBN films were continuous and smooth with no observable pinholes or wrinkles across the entire deposited substrate. They believed that formation of NCBN is due to the random and uncontrolled nucleation of hBN on the dielectric substrate surface with no epitaxial relation, unlike on metal surfaces.

For the CVD process, growth temperature, precursor pressure and hydrogen partial pressure are the key factors to be considered for efficient graphene film production.^[38-43] hBN has been known to exhibit different behaviors, depending on the precursor used.^[32] Controlling the ratio between the boron source and ammonia (NH_3) is critical for obtaining stoichiometric hBN layers and controlling the deposition rate.^[44] Synthesizing a hBN thin film via the pyrolysis of a single precursor such as borazine shows many advantages due to the 1:1 B/N stoichiometry.^[45,46] On the other hand, the use of a mixture of ammonia and diborane as the precursor suggests that the thickness of the grown hBN layers can be controlled by changing the growth temperature and period.^[35] The growth rate of hBN can be decreased by using a powdered precursor such as ammonia borane, which is helpful for obtaining uniform single layers of hBN.^[29] Hydrogen had strong effects when added to the CVD precursor gases, by controlling the in-plane expansion and morphology of the growing hBN domains.^[27]

In addition to the precursor used in the CVD process, there are also many other key factors to be considered for high-

quality hBN growth, as shown in Table 1.

2.4 Other synthesis methods

In addition to the above methods, Nag *et al.*^[50] synthesized single- and few-layer BN sheets by reacting boric acid with different proportions of urea at 900°C. A few-layer BN sample exhibited a surface area of 927 m²/g and high CO₂ uptake, which benefits the preparation of functionalized composite materials. Surface segregation appears to be another feasible method for the large-scale synthesis of hBN. Suzuki *et al.*^[51] proposed a much simpler and safer method, in which the B and N atoms diffuse through the metal film such as Co or Ni, and form thin hBN films by precipitation on both the topmost Co (Ni) surface and at the Co (Ni)/ SiO_2 interface. They believe that the mass transport is caused by grain boundary diffusion.

Xue *et al.*^[52] successfully synthesized large-scale BN nanosheets (BNNSSs) using a ball-milled mixture of NH_4BF_4 and $NaBH_4$ as a novel precursor, under an ammonia atmosphere. This method produced highly crystallized and pure characteristics of the BNNSSs, with an ultrafine hexagonal-sheet structure stacked with a few well-aligned (002) crystal planes. Nakhaii *et al.*^[53] reported the growth of hBN films on Ni foils from elemental B and N using molecular beam epitaxy. Using shorter growth times, they were able to gain insight into the nucleation and growth behavior of hBN before forming a closed film. The morphology of submonolayer islands evolves from ramified and "star"-shaped islands to much larger, smooth, and triangular islands with increasing growth temperature. Wang *et al.*^[54] demonstrated an ion beam sputter deposition (IBSD) method to grow high quality few-layer hBN. Smaller

irregular polygonal hBN domains were formed in pure argon atmosphere, while the larger triangular domains were obtained by introducing hydrogen into the deposition chamber due to the suppressed vertical growth and enhanced lateral growth rates.

3. TRANSFER OF 2D HBN

All of the synthesis methods described in the previous section attempt to improve the quality of 2D hBN films and to find large scale production techniques. However, once synthesized, the 2D hBN material must be exfoliated or transferred from the substrate upon which it was grown to its final carrier substrate, for instance a silicon wafer or a substrate for the formation of a boron nitride based van der Waals heterostructure for future use in electronic devices. In this section the main methods for the transfer of 2D hBN films are reviewed.

As in the case of graphene transfer as shown in Fig. 5, the most widely used method for transferring boron nitride films is the polymer-supported transfer method.^[56] For hBN films grown on copper foil, as an example, the transfer process consists of three essential steps^[18]: (i) adhesion of a polymer supporting film to the boron nitride on the copper foil; (ii) backside etching to remove the catalyst copper layer; and (iii) release of the hBN layers and transfer onto a target substrate.

Liang *et al.*^[57] developed a “modified RCA clean” process for the transfer (Fig. 6), including the two standard cleans (SC1: H₂O/H₂O₂/NH₄OH, and SC2: H₂O/H₂O₂/HCl), but in

reverse order, by use of which either Cu or Fe contamination can be thoroughly reduced.

Recently, an improved transfer technique (Fig. 7) based on mechanical separation of the catalyst film by using H₂ bubbles during H₂O electrolysis has been developed.^[32,58-61] After CVD growth, a catalyst substrate with the hBN grown on it was first spin-coated with polymethyl methacrylate (PMMA) followed by curing. Then it was dipped into a NaOH aqueous solution and used as the cathode of an electrolysis cell with a constant current supply. The PMMA/hBN layer becomes detached from the substrate after tens of seconds as a result of the formation of a large number of H₂ bubbles at the interface between the hBN and substrate. This method allows the reuse of the catalyst film, and reduces the introduction of impurities during etching and cleaning processes. De la Rosa *et al.*^[62] reported a convenient way of handling graphene films during transfer by using a semi-rigid plastic frame in combination with the polymer layer, thereby avoiding wrinkles and holes in the graphene film. Similar methods could probably be used for the transfer of BN films.

However, all of the transfer methods for two-dimensional hBN films result in them becoming contaminated by polymer residue, which will increase scattering of low frequency phonons in thin hBN samples. Insun *et al.*^[63] found that the thermal conductivity at room temperature is decreased by the presence of a polymer residue layer on the sample surface. As the sample thickness decreases, the thermal conductivity decreases because of increasing phonon scattering by polymer residues, which is more pronounced at low

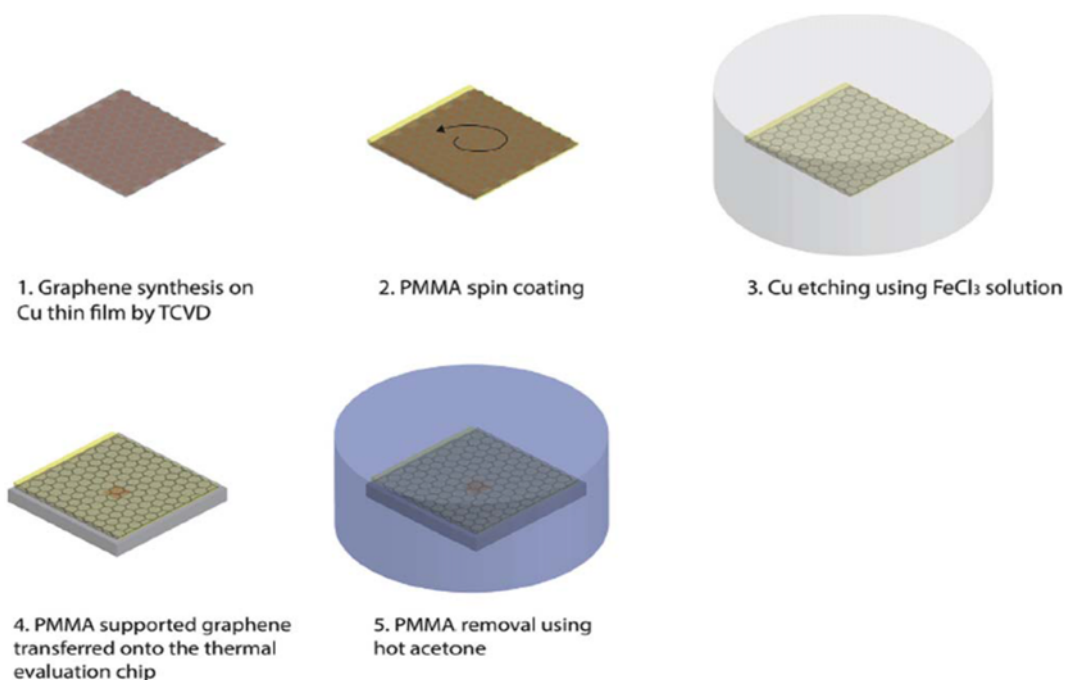


Fig. 5. schematic of grapheme transfer process (Taken from ref. 55. Reproduced by permission of Elsevier Science & Technology Journals).

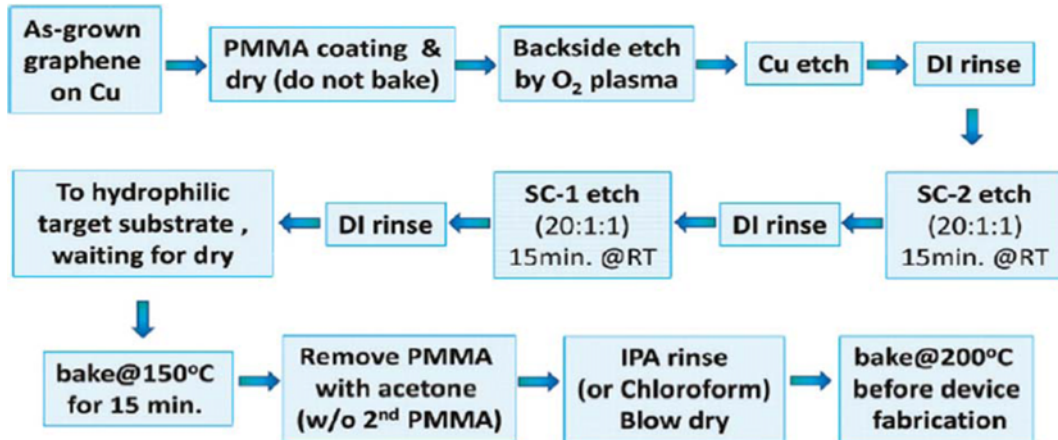


Fig. 6. “Modified RCA clean” graphene transfer process flow (Taken from ref. 57. Reproduced by permission of American Chemical Society).

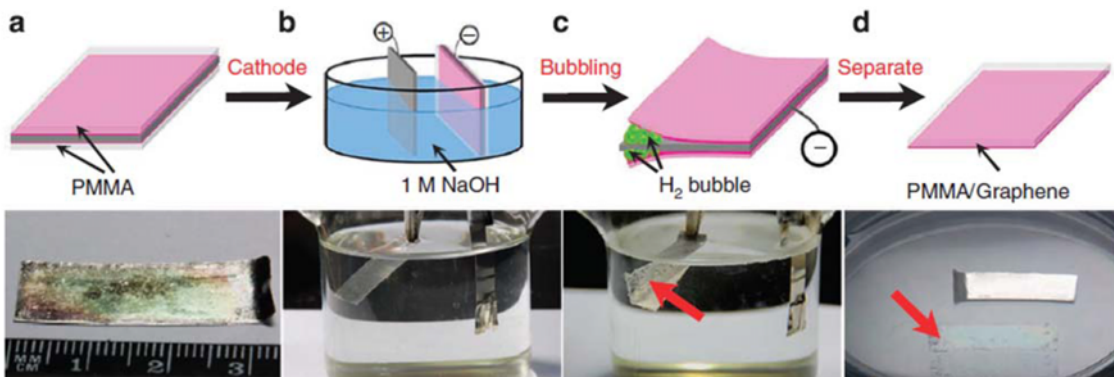


Fig. 7. Illustration of the bubbling transfer process of graphene from a Pt substrate (Taken from ref. 59. Reproduced by permission of Nature Publishing Group).

temperatures or for low-frequency phonons. Wen *et al.*^[33] performed the electrochemical bubble treatment immediately after the spin coating of PMMA without any baking. After hBN was nondestructively separated from the copper substrate within 1 min, the PMMA was totally dissolved by methylene chloride without the aid of any thermal annealing. They believed that this optimized method will result in ultraclean monolayer hBN.

In addition to the above methods, hBN can be transferred by a nondestructive lithography method^[64] that has the additional advantage for organic field effect transistors (OFETs) of avoiding damage from organic solvents. The hBN flakes were prepared by the mechanical exfoliation method on a polydimethylsiloxane (PDMS) stamp which had a step-free and clean surface. Then they were transferred onto the channel area of a rubrene single crystal using a three-axis micro-manipulator. The authors believe that this straightforward and lithography-free fabrication method enabled them to produce high performance OFETs.

4. APPLICATION OF 2D HBN IN ELECTRON-ICS MANUFACTURING

One of the most attractive properties of 2D hBN for electronic applications is that its lattice constant and structure is similar to that of graphene. Furthermore, it has large optical phonon modes and a large electrical bandgap, as well as an atomically smooth surface almost free of dangling bonds and charge traps.^[6,65] For both two-dimensional boron nitride films themselves, and for 2D hBN based van der Waals heterostructures there is a large number of applications in electronics manufacturing. In this section, fabrication of 2D hBN based van der Waals heterostructures and 2D hBN based applications in tunnel devices, transistors, interconnect, as well as packaging are reviewed.

4.1 Fabrication of 2D hBN based van der Waals heterostructures

Van der Waals heterostructures are artificial materials

assembled in a specific sequence, like building blocks. These heterostructures are made by stacking different two-dimensional layers on top of each other, as shown in Fig. 8. In-plane stability is provided by the strong covalent bonds and although van-der-Waals-like forces are relatively weak they are sufficiently strong for keeping the stack together.^[1] Taking a van der Waals heterostructure composed of a monolayer graphene flake coupled to a rotationally aligned hexagonal boron nitride substrate as an example, the spatially varying interlayer atomic registry results in both a local breaking of the carbon sublattice symmetry and a long-range moiré superlattice potential in the graphene. This interplay between short- and long-wavelength effects results in a band structure and an unexpectedly large band gap at charge neutrality.^[66] Recently, the fabrication of multilayer van der Waals heterostructures has been developed from being theoretical scientific proposals to experimental verification. Such heterostructures provide higher electronic

quality such as superior mobilities and carrier inhomogeneities for lateral graphene devices,^[6,67] and they will also allow a conceptually new degree of flexibility in designing electronic, optoelectronic, micromechanical and other devices.^[68-71]

At the time of reviewing this topic, only a few groups have reported van der Waals heterostructures made from films with more than two layers.^[1] Dean *et al.*^[6] reported on the fabrication and characterization of high-quality exfoliated mono- and bilayer graphene devices on single-crystal hBN substrates by using a mechanical transfer process, as shown in Fig. 9. Graphene devices on hBN substrates have mobilities and carrier inhomogeneities that are almost an order of magnitude better than devices on SiO₂. These devices also show reduced roughness, intrinsic doping and chemical reactivity. Preservation of high mobility in dual-gated devices may be achieved by fabricating hBN-graphene-hBN stacks using a double-transfer technique shown in Fig. 9.

Haigh *et al.*^[72] presented an example of a more sophisticated

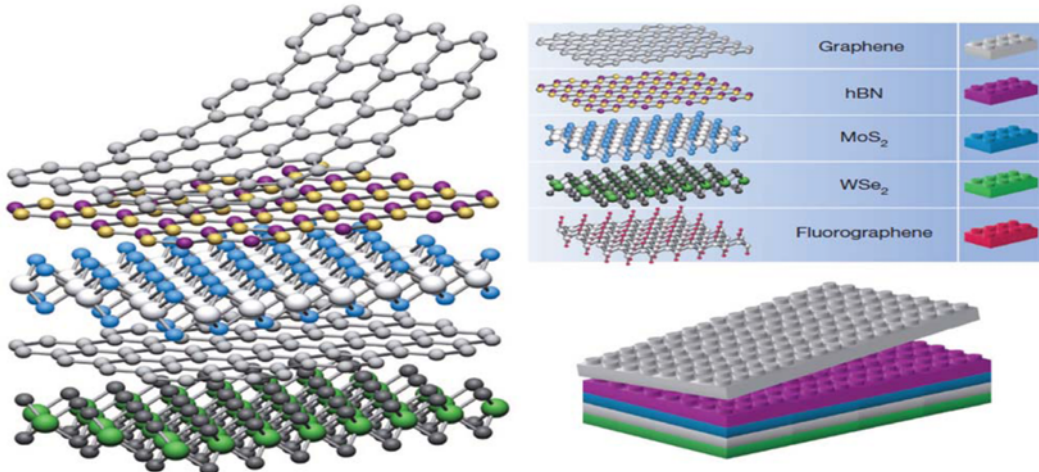


Fig. 8. Building van der Waals heterostructures (Taken from ref. 1. Reproduced by permission of Nature Publishing Group).

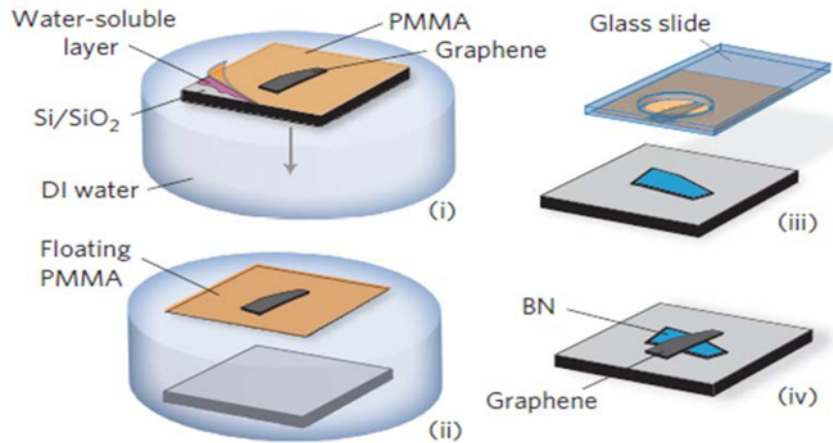


Fig. 9. Schematic illustration of the transfer process used to fabricate graphene-on-BN devices (Taken from ref. 6. Reproduced by permission of Nature Publishing Group).

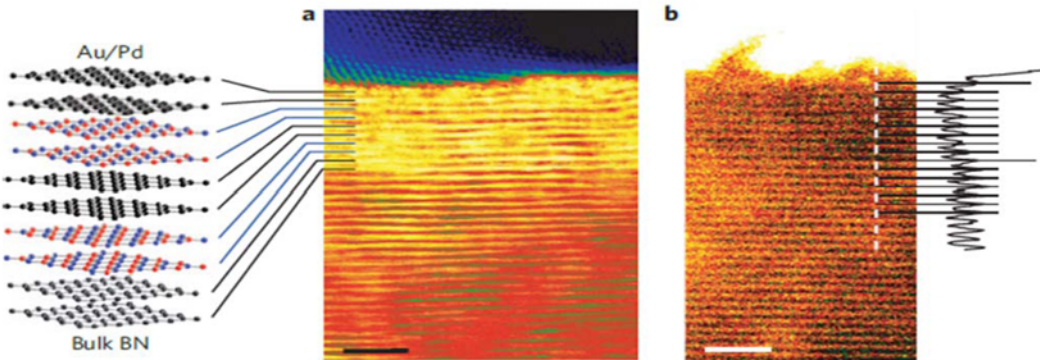


Fig. 10. Graphene-BN superlattice. (a) Bright-field cross-sectional STEM of a stack of graphene and hBN bilayers with the layer sequence schematically shown on the left. (b) HAADF STEM image of the same superlattice with an intensity line profile of length 7 nm and integration width 5 nm plotted to the right (Taken from ref. 72. Reproduced by permission of Nature Publishing Group).

heterostructure as shown in Fig. 10. This is a van der Waals heterostructure comprised of several graphene bilayers separated by hBN bilayers. The stack begins with a thick (~50 nm) hBN flake deposited on top of an oxidized Si wafer. Each subsequent layer is prepared on a separate wafer, delaminated from the surface and transferred on top of the target crystal. The freshly deposited layer can then be shaped by reactive plasma etching and annealed (300°C in Ar/H₂) to remove processing residues. The measurements proved that the contamination inevitably present on top of 2D crystals and trapped during their assembly segregates into isolated pockets, leaving the buried interfaces clean and atomically flat, which is good for their electronic quality.

Liu *et al.*^[73] demonstrated direct CVD growth of hBN on highly oriented pyrolytic graphite and on mechanically exfoliated graphene. They also showed large area growth of graphene/hBN stacks by using a two-step CVD process. The graphene/hBN film is uniform and continuous and can be transferred onto different substrates for further characterization and device fabrication. Wang *et al.*^[74] reported direct CVD growth of graphene on CVD-grown hBN films, to obtain a large area pristine graphene/hBN interface, which is demanded for graphene-based devices. The devices exhibited superior carrier mobility and suppression of charged impurities. Garcia *et al.*^[75] demonstrated molecular beam epitaxy (MBE) growth of nanometer-sized domains of graphene on boron nitride flakes. The growth is governed by the high mobility of the carbon atoms on the hBN surface, in a manner that is consistent with Van der Waals epitaxy. The successful growth of graphene layers depends on the substrate temperature, but is independent of the incident flux of carbon atoms. Gao *et al.*^[76] developed a novel temperature-triggered reaction route in CVD process to achieve the selective growth of hBN-G and G/hBN heterostructures on Cu foils. Their work demonstrated the chemical designability of CVD process for deliberate control of graphene and hBN heterostructures. Sharma *et al.*^[77] developed a H₂-induced etching process to

introduce a triangular hole in a triangular-shaped chemical vapor deposited individual hBN crystal. The etching mechanism was isotropic or anisotropic depending on annealing temperature. The etching process and the well-defined triangular hole formation is potentially a significant platform for fabricating planar heterostructures of graphene or other two-dimensional materials.

In addition to the hBN-graphene heterostructures already described, functionalized 2D hBN can also be used to obtain custom-made materials for electronics manufacturing. Layers of atomically mixed boron-carbon-nitrogen (BCN) structures have band gaps and show electronic properties that are halfway between those of pure graphene and hBN.^[5] Ci *et al.*^[78] used a thermal catalytic CVD method to synthesize large-area atomic layers of hBNC materials, consisting of hybridized, randomly distributed domains of boron nitride and carbon phases with compositions ranging from pure BN to pure graphene (Fig. 11). Such a method would enable the development of bandgap-engineered materials with properties that are distinct from those of graphene and hBN for applications in electronics and optics.

4.2 2D hBN based substrates and gate dielectric

Most graphene transistors fabricated today are found either on a silicon substrate with a thin SiO₂ film on top, or on a SiC substrate.^[79,80] However, none of these substrates are ideal for graphene transistors. The quality of graphene on SiO₂ is limited by scattering from charged surface states and impurities, substrate surface roughness and SiO₂ surface optical phonons.^[81-88] On the other hand, the quality of graphene on SiC is deteriorated by charge carrier scattering due to the rough, terraced SiC surface limiting any device performance.^[89] Hence, in order to take full advantage of the ultra-high mobility demonstrated for graphene, a more suitable substrate, like boron nitride should be used. The bandgap (5.97 eV) of hBN ($\epsilon \sim 3 - 4$) as well as its dielectric properties and breakdown field ($E_{BD} \sim 0.7$ V/nm) compare

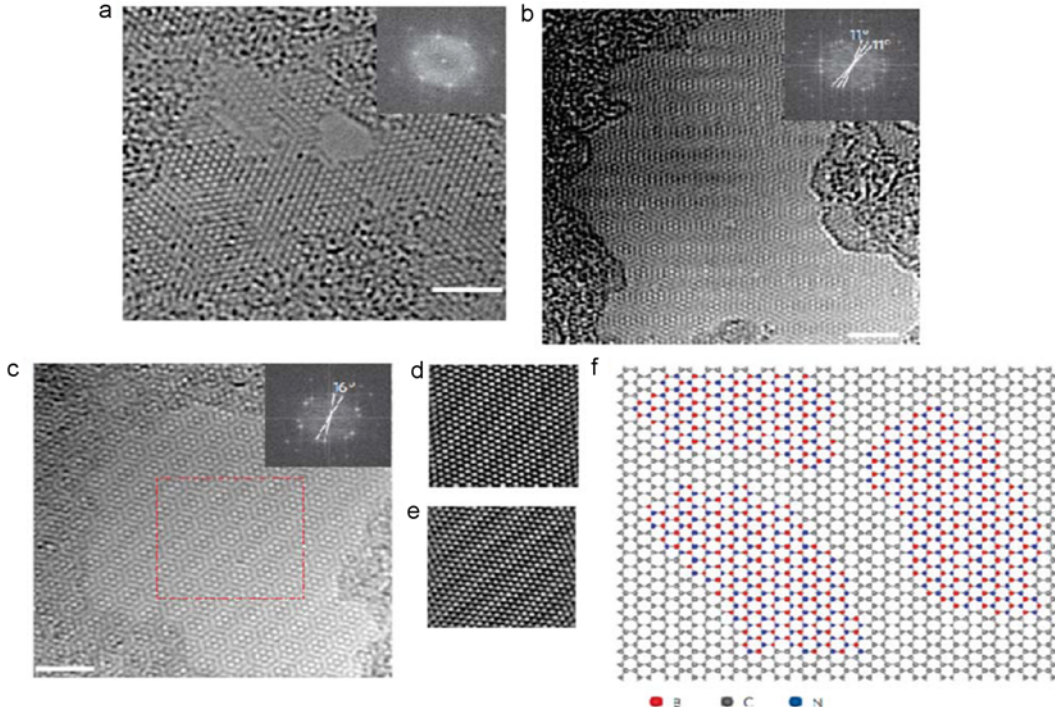


Fig. 11. Atomic HRTEM images of hBNC film. (a) A single-layer region exposed a nearby hole in the film, (b, c) atomic-scale Moiré pattern from different regions, (d, e) two individual atomic layers reconstructed by masking the FFT pattern from the area in (c) (red line), (f) atomic model of the hBNC film showing hybridized hBN and graphene domains (Taken from ref. 78. Reproduced by permission of Nature Publishing Group).

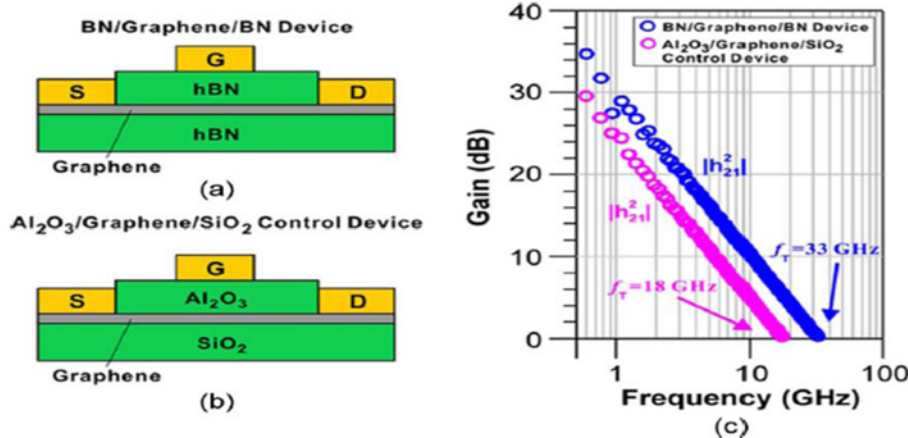


Fig. 12. (a) Schematic of the BN/graphene/BN device structure, (b) schematic of the $\text{Al}_2\text{O}_3/\text{Graphene}/\text{SiO}_2$ control device structure, (c) comparison of the BN/graphene/BN device with the control device in terms of maximum f_T (Taken from ref. 68. Reproduced by permission of Institute of Electrical and Electronic Engineers).

favorably with SiO_2 . The thermal conductivity of hBN, which is 600 times higher than that of silicon dioxide, is also advantageous for lateral heat spreading in field-effect transistor (FET) circuits.^[88]

Wang *et al.*^[68] demonstrated the first BN/graphene/BN radio-frequency FET, where hBN was used both as the substrate and gate dielectric, while a bilayer graphene was

used as the channel material (Fig. 12); this allows for much higher mobility and carrier velocity than those obtained for SiO_2/Si substrates and Al_2O_3 gate dielectrics. Britnell *et al.*^[90] investigated the electronic properties of ultrathin hBN crystalline layers with different conducting materials on either side of the barrier layer (Fig. 13). The tunnel current depends exponentially on the number of hBN atomic layers,

down to monolayer thickness. Their results demonstrated that atomically thin hBN acts as a defect-free dielectric with a high breakdown field. It offers great potential for applications in tunnel devices.^[90,91]

The technology of transferring atomically thin membranes from substrate to substrate while maintaining the integrity of the graphene and the quality of the electronic system opens up a number of experimental directions which were not possible before. Dean *et al.*^[92] showed a few possible geometries for both technological and fundamental applications, shown Fig. 14, including dual gated graphene devices for capacitance measurements, thin hBN FET structure, designed for high transconductance, and dual gated, double layer graphene structure with independence contacts to the two graphene layers.

4.3 2D hBN based insulating layers in packaging applications

Recently, graphene has emerged as a front runner as a potential interconnect material in future post-copper era due to its excellent material and electrical properties, including a high breakdown current density and robustness to electromigration.^[93] While graphene exhibits current densities about 100 times larger than that of copper, its atomically-thin nature limits the current handling capability. Attempts have been made to further enhance the current handling capability by stacking graphene layers to create a layer-by-layer structure.^[94] While each monolayer serves as a conduction channel, interlayer scattering is responsible for the observed non-linear behavior in resistivity when more graphene layers are added.^[95]

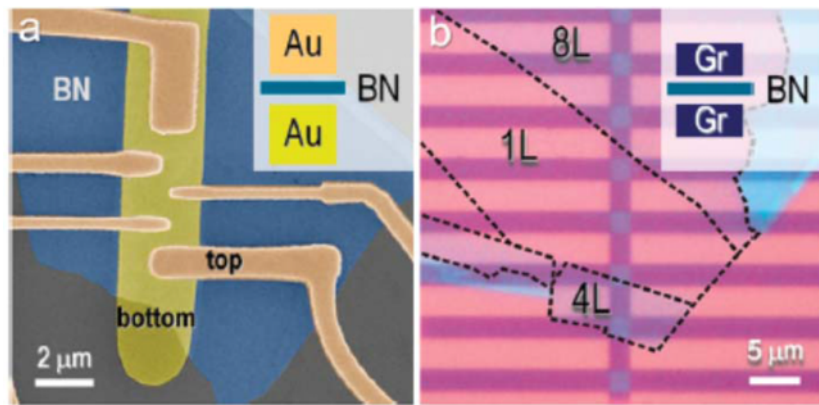


Fig. 13. Micrographs of two of tunnel devices. (a) A SEM micrograph of a Au/BN/Au device, (b) an optical image of a graphite/BN/graphite device. Crossing the top graphite layer forms several tunneling junctions with different thicknesses of BN (Taken from ref. 90. Reproduced by permission of American Chemical Society).

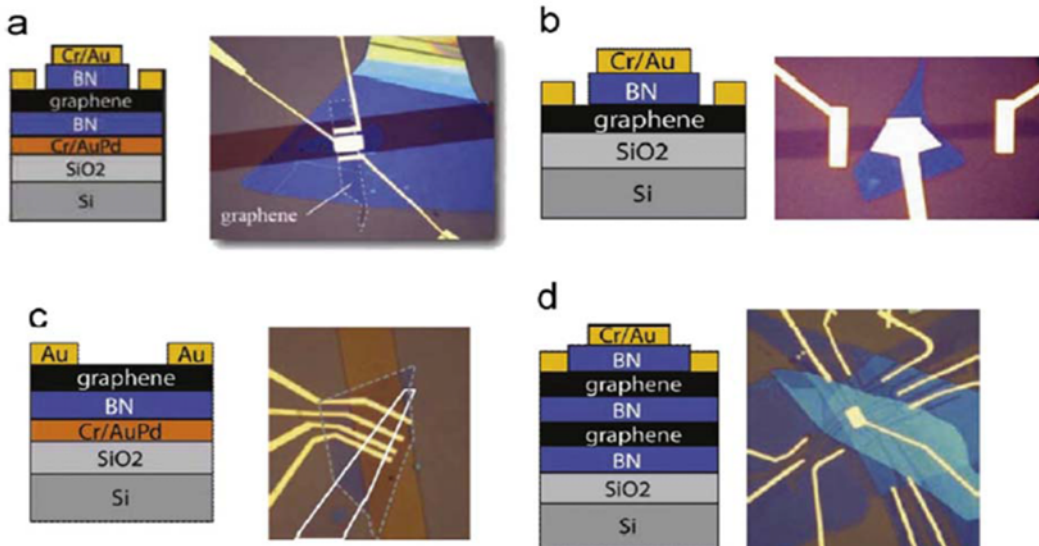


Fig. 14. Sample device geometries enabled by the combination of hBN gate dielectrics and the aligned transfer process. (a, b) Dual gated graphene devices for capacitance measurements, (c) thin-film hBN FET structure, designed for high transconductance, (d) dual gated, double layer graphene structure with independence contacts to the two graphene layers. Interlayer Coulomb drag and tunneling measurements are now possible between clean graphene monolayers (Taken from ref. 92. Reproduced by permission of Elsevier).

Due to its high bandgap and excellent in-plane thermal conductivity, hBN is both an excellent electrical insulator and a thermal conductor. Mayorov *et al.*^[67] reported that devices made from hBN encapsulated graphene exhibit a pronounced negative bend resistance and an anomalous Hall effect. The encapsulation (Fig. 15) was shown to eliminate any interference from ambient adsorbents, leading to a stable electrical behavior without any time-dependent parameter drift.^[96] Jain *et al.*^[97] performed studies on electrical conduction and reliability of dual-layer graphene wire heterostack containing thin hBN barrier layers. Significant improvement in interconnect metrics, including current-carrying capacity and maximum power density at breakdown, were observed compared with monolayer and stacked bilayer graphene. Han *et al.*^[98] demonstrated the deposition of a high-k dielectric material on graphene using hBN nanosheets as a buffer layer, which facilitated the growth of high-quality Al₂O₃ by atomic layer deposition (ALD). In addition, the presence of an hBN layer on top of the graphene surface effectively prevents possible oxidation during the ALD deposition of Al₂O₃.

Another important challenge in modern electronic devices development is the thermal management. For the emerging package integration levels such as many-core architectures and three-dimensional chip stacking, serious thermal challenges call for new materials with high thermal conductivity. Required cooling should be delivered to keep the hottest region of a die under its stated temperature threshold.^[99] Due to the absence of interlayer phonon scattering, the thermal conductivity of an ideal 2D system, such as suspended single layer graphene or hBN, is expected to be higher than the basal-plane values of their three-dimensional stacks, namely, graphite and bulk hBN.^[100] However, in experimental studies, a considerable reduction in the basal-plane thermal conductivity has been found for both graphene and hBN supported on or encased in an amorphous material or contaminated by polymer residue,^[101-104] as shown in Fig. 16.

Yan *et al.*^[105] reported that the use of exfoliated graphene as a lateral heat spreader on top of a high-power transistor

reduced the maximum device temperature by almost 20°C; thereby they predict this material will extend transistor lifetime about one order of magnitude. However, it is difficult to control the number of layers, their size and location of the graphene when it is mechanically exfoliated using Scotch tape. Gao *et al.*^[55] used monolayer graphene synthesized on copper foil by thermal chemical vapor deposition (CVD), a method that offers better control of the number of graphene monolayers, as a lateral heat spreader. Using a thermal test chip they showed that the temperature of a metal resistor hot spot could be lowered from 121°C to 108°C at a heat flux density of 430 W/cm² due to the graphene lateral heat spreader.

However, the authors found that, graphene is not only thermally conductive, but also electrically conductive, and therefore it must be electrically insulated from the hot spot

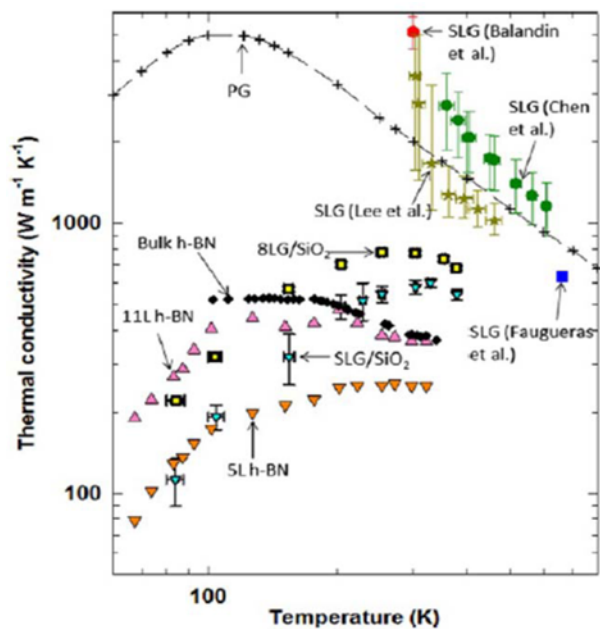


Fig. 16. Comparison of reported experimental thermal conductivity values of graphite, graphene, and hBN (Taken from ref. 100. Reproduced by permission of American Chemical Society).

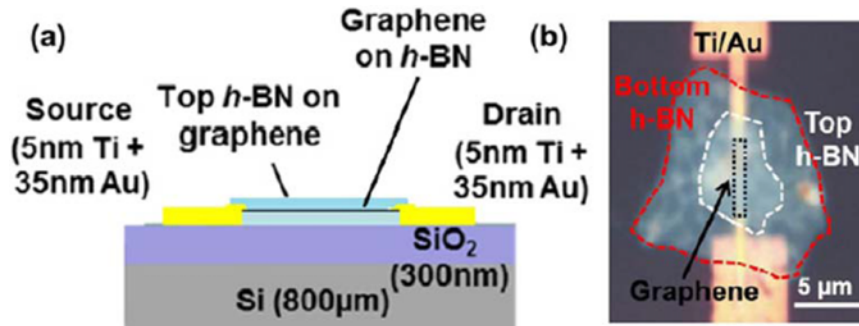


Fig. 15. Encapsulated graphene interconnect: (a) schematic cross-section view of the hBN/graphene/hBN heterostructure. (b) optical microscope image showing the top view of a graphene interconnect wire (Taken from ref. 96. Reproduced by permission of Institute of Physics Publishing).

using silicon dioxide, SiO_2 , or other insulators most often of poor thermal conductance. For large insulator thicknesses the cooling effect of the heat sink/spreader will be severely reduced. Therefore, the ideal solution would be a high-quality electrically-insulating material with a high thermal conductance. They utilized a 2D hBN film in power chips as both an insulating layer and a heat spreader for local hotspots with high heat flux. Resistance temperature detectors (RTDs) and infrared thermal imagers are both used to measure the temperature of a hotspot generated from a heated resistor on a thermal test chip.

Bao *et al.*^[106] compared the heat dissipation capacity of single-layer hBN growth by CVD with micron hBN film, the results showed a better cooling efficiency in the single-layer hBN film. To avoid the impact of the polymer residue on the thermal conductivity, the liquid-phase exfoliation method is selected to synthesize the hBN materials. The use of a hBN heat spreader film was found to reduce the hotspot temperature by approximately 20°C compared to the bare quartz chip for heat flux at about 640 W/cm² as shown in Fig. 17.^[107] In addition, in follow up work, to simplify the subsequent cleaning process, a solvent consisting of ethanol and DI water was used to produce few-layer hBN flakes. The products were then functionalized with a graphene dispersion to form the films easily and achieve better contact with the surface of the hot spot test structure. At the same time, the thermal conductivity of the samples might have been increased.

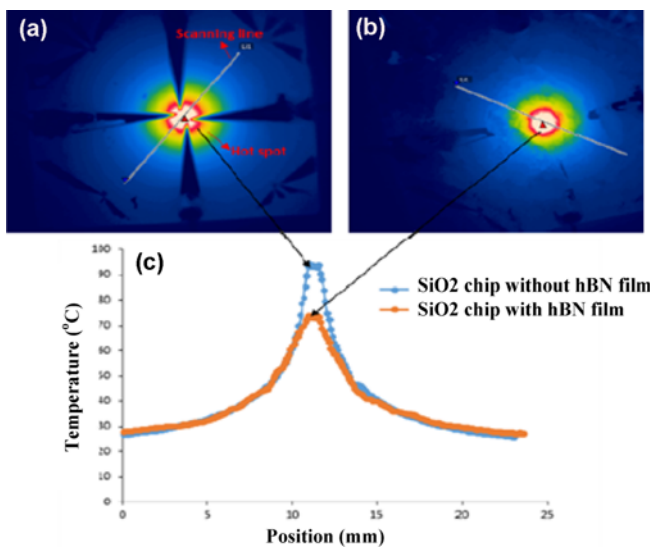


Fig. 17. Hot spot temperature with and without boron nitride heat spreader. The images show the thermal image of the temperature distribution on the backside of the test chip resulting from a 640 W/cm² heat flux for (a) the bare chip and (b) the hBN heat spreader chip, while (c) shows the temperature along the test line (Taken from ref. 107).

5. CONCLUSIONS

2D hBN possesses excellent electrical, thermal and mechanical properties. Therefore, this material is a candidate for many applications in electronics. This paper has reviewed the state of the art of synthesis, transfer, and application of such two-dimensional films. In particular, two main applications have been considered, namely as a substrate layer and gate dielectric for tunnel devices or graphene transistors and as an insulating layer for graphene interconnects and encapsulation. The synthesis and transfer of 2D hBN for specific applications have also been described.

As is typical for two-dimensional materials, there are many technical difficulties to be overcome when it comes to synthesis, transfer and application of hexagonal boron nitride films. As a result of the poor stability of atomically thin films compared to their three-dimensional counterparts, the total number of two-dimensional materials should be relatively small. Another important consideration is interfacial contamination.^[11] If isolated two-dimensional materials are stacked together, the surface contamination becomes trapped in between layers, which impacts on performance and makes it difficult to reproducibly manufacture the films. Research on this topic still remains at an early stage of development and is showing some promise. The possibility of combining 2D boron nitride films with other materials promises to dramatically improve performance of future electronic devices and systems. Exciting results are expected to emerge from this field as it rapidly evolves over the next few years.

ACKNOWLEDGEMENTS

This work was supported by the National Natural Science Foundation of China (51272153, 61574088, 11272192), Shanghai Science and Technology Program (12JC1403900), Shanghai Jiading Governmental program and Anhui Natural Science Project (KJHS2015B10, KJHS2015B08, KJHS2015B02). We also acknowledge the program from the Swedish Board for Strategic Research (SSF) “Scalable Nanomaterials and Solution Processable Thermoelectric Generators” with the contract No. EM11-0002, the SSF program “Carbon Based 3D GaN high speed electronic system” with the contract No: SE13-0061 and the EU FP7 program “Nanotherm”. This work is also carried out within the Sustainable Production Initiative and the Production Area of Advance at Chalmers.

REFERENCES

1. A. K. Geim and I. V. Grigorieva, *Nature* **499**, 419 (2013).
2. K. S. Novoselov, V. I. Fal'ko, L. Colombo, P. R. Gellert, M. G. Schwab, and K. Kim, *Nature* **490**, 192 (2012).
3. A. A. Balandin, *Nat. Mater.* **10**, 569 (2011).

4. M. Osada and T. Sasaki, *Adv. Mater.* **24**, 210 (2012).
5. M. Xu, T. Liang, M. Shi, and H. Chen, *Chem. Rev.* **113**, 3766 (2013).
6. C. R. Dean, A. F. Young, I. Meric, C. Lee, L. Wang, S. Sorgenfrei, K. Watanabe, T. Taniguchi, P. Kim, K. L. Shepard, and J. Hone, *Nature Nanotech.* **5**, 722 (2010).
7. Y. Chen, J. Zou, S. J. Campbell, and G. L. Caer, *Appl. Phys. Lett.* **84**, 2430 (2004).
8. D. Golberg, P. M. F. J. Costa, O. Lourie, M. Mitome, X. Bai, K. Kurashima, C. Zhi, C. Tang, and Y. Bando, *Nano Lett.* **7**, 2146 (2007).
9. C. W. Chang, D. Okawa, A. Majumdar, and A. Zettl, *Science* **314**, 1121 (2006).
10. D. Golberg, Y. Bando, Y. Huang, T. Terao, M. Mitome, C. Tang, and C. Zhi, *ACS Nano* **4**, 2979 (2010).
11. Y. Wang, Z. Shi, and J. Yin, *J. Mater. Chem.* **21**, 11371 (2011).
12. D. Pacilé, J. C. Meyer, Ç. Ö. Girit, and A. Zettl, *Appl. Phys. Lett.* **92**, 133107 (2008).
13. J. N. Coleman, M. Lotya, A. O'Neill, S. D. Bergin, P. J. King, U. Khan, K. Young, A. Gaucher, S. De, R. J. Smith, I. V. Shvets, S. K. Arora, G. Stanton, H.-Y. Kim, K. Lee, G. T. Kim, G. S. Duesberg, T. Hallam, J. J. Boland, J. J. Wang, J. F. Donegan, J. C. Grunlan, G. Moriarty, A. Shmeliov, R. J. Nicholls, J. M. Perkins, E. M. Grieveson, K. Theuwissen, D. W. McComb, P. D. Nellist, and V. Nicolosi, *Science* **331**, 568 (2011).
14. R. J. Smith, P. J. King, M. Lotya, C. Wirtz, U. Khan, S. De, A. O'Neill, G. S. Duesberg, J. C. Grunlan, G. Moriarty, J. Chen, J. Wang, A. I. Minett, V. Nicolosi, and J. N. Coleman, *Adv. Mater.* **23**, 3944 (2011).
15. K.-G. Zhou, N.-N. Mao, and H.-X. Wang, *Angew. Chem. Int. Edit.* **50**, 10839 (2011).
16. J. H. Warner, M. H. Rümmeli, A. Bachmatiuk, and B. Büchner, *ACS Nano* **4**, 1299 (2010).
17. C. Zhi, Y. Bando, C. Tang, H. Kuwahara, and D. Golberg, *Adv. Mater.* **21**, 2889 (2009).
18. S. Bae, H. Kim, Y. Lee, X. Xu, J. S. Park, Y. Zheng, J. Balakrishnan, T. Lei, H. R. Kim, Y. I. Song, Y. J. Kim, K. S. Kim, B. Ozayilmaz, J. H. Ahn, B. H. Hong, and S. Iijima, *Nature Nanotech.* **5**, 574 (2010).
19. T. Yamada, M. Ishihara, J. Kim, M. Hasegawa, and S. Iijima, *Carbon* **50**, 2615 (2012).
20. K. S. Novoselov, A. K. Geim, S. V. Morozov, D. Jiang, Y. Zhang, S. V. Dubonos, I. V. Grigorieva, and A. A. Firsov, *Science* **306**, 666 (2004).
21. L. H. Li, Y. Chen, G. Behan, H. Zhang, M. Petracic, and A. M. Glushenkova, *J. Mater. Chem.* **21**, 11862 (2011).
22. W. Q. Han, L. Wu, Y. Zhu, and T. T. Kenji, *Appl. Phys. Lett.* **93**, 223103 (2008).
23. Y. Lin, T. V. Williams, T.-B. Xu, W. Cao, H. E. Elsayed-Ali, and J. W. Connell, *J. Phys. Chem. C* **115**, 2679 (2011).
24. Y. Zhao, C. Hu, Y. Hu, H. Cheng, G. Shi, and L. Qu, *Angew. Chem.-Int. Edit.* **51**, 11371 (2012).
25. Y. Lin, T. V. Williams, W. Cao, H. E. Elsayed-Ali, and J. W. Connell, *J. Phys. Chem. C* **114**, 17434 (2010).
26. G.-X. Ni, Y. Zheng, S. Bae, C. Y. Tan, O. Kahya, J. Wu, B. H. Hong, K. Yao, and B. Özayilmaz, *ACS Nano* **6**, 3935 (2012).
27. P. Sutter, J. Lahiri, P. Albrecht, and E. Sutter, *ACS Nano* **5**, 7303 (2011).
28. E. Ćavar, R. Westerström, A. Mikkelsen, E. Lundgren, A. S. Vinogradov, M. L. Ng, A. B. Preobrajenski, A. A. Zakharov, and N. Mårtensson, *Surf. Sci.* **602**, 1722 (2008).
29. K. K. Kim, A. Hsu, X. Jia, S. M. Kim, Y. Shi, M. Hofmann, D. Nezich, J. F. Rodriguez-Nieva, M. Dresselhaus, T. Palacios, and J. Kong, *Nano Lett.* **12**, 161 (2012).
30. L. Song, L. Ci, H. Lu, P. B. Sorokin, C. Jin, J. Ni, A. G. Kvashnin, D. G. Kvashnin, J. Lou, B. I. Yakobson, and P. M. Ajayan, *Nano Lett.* **10**, 3209 (2010).
31. F. Mueller and S. Grandthyll, *Surf. Sci.* **617**, 207 (2013).
32. G. Kim, A.-R. Jang, H. Y. Jeong, Z. Lee, D. J. Kang, and H. S. Shin, *Nano Lett.* **13**, 1834 (2013).
33. Y. Wen, X. Shang, J. Dong, K. Xu, J. He, and C. Jiang, *Nanotechnology* **26**, 275601 (2015).
34. K. H. Lee, H. J. Shin, and J. Lee, *Nano Lett.* **12**, 714 (2012).
35. A. Ismach, H. Chou, D. A. Ferrer, Y. Wu, S. McDonnell, H. C. Floresca, A. Covacevich, C. Pope, R. Piner, M. J. Kim, R. M. Wallace, L. Colombo, and R. S. Ruoff, *ACS Nano* **6**, 6378 (2012).
36. K. H. Lee, H. J. Shin, B. Kumar, H. S. Kim, J. Lee, R. Bhatia, S. H. Kim, I. Y. Lee, H. S. Lee, G. H. Kim, J. B. Yoo, J. Y. Choi, and S. W. Kim, *Angew. Chem. Int. Ed.* **53**, 11493 (2014).
37. R. Y. Tay, S. H. Tsang, M. Loeblein, W. L. Chow, G. C. Loh, J. W. Toh, S. L. Ang, and E. H. T. Teo, *Appl. Phys. Lett.* **106**, 101901 (2015).
38. T. Kobayashi, M. Bando, N. Kimura, K. Shimizu, K. Kadono, N. Umezu, K. Miyahara, S. Hayazaki, S. Nagai, Y. Mizuguchi, Y. Murakami, and D. Hobara, *Appl. Phys. Lett.* **102**, 023112 (2013).
39. I. Vlassiouk, S. Smirnov, I. Ivanov, P. F. Fulvio, S. Dai, H. Meyer, M. Chi, D. Hensley, P. Datskos, and N. V. Lavrik, *Nanotechnology* **22**, 275716 (2011).
40. L. Liu, H. Zhou, R. Cheng, Y. Chen, Y.-C. Lin, Y. Qu, J. Bai, I. A. Ivanov, G. Liu, Y. Huang, and X. Duan, *J. Mater. Chem.* **22**, 1498 (2012).
41. X. Li, C. W. Magnuson, A. Venugopal, R. M. Tromp, J. B. Hannon, E. M. Vogel, L. Colombo, and R. S. Ruoff, *J. Am. Chem. Soc.* **133**, 2816 (2011).
42. X. Li, C. W. Magnuson, A. Venugopal, J. An, J. W. Suk, B. Han, M. Borysiak, W. Cai, A. Velamakanni, Y. Zhu, L. Fu, E. M. Vogel, E. Voelk, L. Colombo, and R. S. Ruoff, *Nano Lett.* **10**, 4328 (2010).
43. I. Vlassiouk, M. Regmi, P. Fulvio, S. Dai, P. Datskos, G. Eres, and S. Smirnov, *ACS Nano* **5**, 6069 (2011).

44. Y. Shi, C. Hamsen, X. Jia, K. K. Kim, A. Reina, M. Hofmann, A. L. Hsu, K. Zhang, H. Li, Z.-Y. Juang, M. S. Dresselhaus, L.-J. Li, and J. Kong, *Nano Lett.* **10**, 4134 (2010).
45. A. Nagashima, N. Tejima, Y. Gamou, T. Kawai, and C. Oshima, *Surf. Sci.* **357**, 307 (1996).
46. M. Corso, W. Auwärter, M. Muntwiler, A. Tamai, T. Greber, and J. Osterwalder, *Science* **303**, 217 (2004).
47. Y. Song, C. Zhang, B. Li, D. Jiang, G. Ding, H. Wang, and X. Xie, *Appl. Surf. Sci.* **313**, 647 (2014).
48. F. Orlando, P. Lacovig, L. Omiciuolo, N. G. Apostol, R. Larciprete, A. Baraldi, and S. Lizzit, *ACS Nano* **8**, 12063 (2014).
49. M. S. Bresnahan, G. R. Bhimanapati, K. Wang, D. W. Snyder, and J. A. Robinson, *ACS Appl. Mater. Interfaces* **6**, 16755 (2014).
50. A. Nag, K. Raidongia, K. P. S. S. Hembram, R. Datta, U. V. Waghmare, and C. N. R. Rao, *ACS Nano* **4**, 1539 (2010).
51. S. Suzuki, R. M. Pallares, and H. Hibino, *J. Phys. D: Appl. Phys.* **45**, 385304 (2012).
52. Y. Xue, X. Jin, Y. Fan, R. Tian, X. Xu, J. Li, J. Lin, J. Zhang, L. Hu, and C. Tang, *Polym. Compos.* **35**, 1707 (2014).
53. S. Nakhaie, J. M. Wofford, T. Schumann, U. Jahn, M. Ramsteiner, M. Hanke, J. M. J. Lopes, and H. Riechert, *Appl. Phys. Lett.* **106**, 213108 (2015).
54. H. Wang, X. Zhang, J. Meng, Z. Yin, X. Liu, Y. Zhao, and L. Zhang, *Small* **11**, 1542 (2015).
55. A. I. Oliva-Avilés, F. Avilés, V. Sosa, and G. D. Seidel, *Carbon* **61**, 342 (2013).
56. J. Kang, D. Shin, S. Bae, and B. H. Hong, *Nanoscale* **4**, 5527 (2012).
57. X. Liang, B. A. Sperling, I. Calizo, G. Cheng, C. A. Hacker, Q. Zhang, Y. Obeng, K. Yan, H. Peng, Q. Li, X. Zhu, H. Yuan, A. R. H. Walker, Z. Liu, L. Peng, and C. A. Richter, *ACS Nano* **5**, 9144 (2011).
58. Y. Wang, Y. Zheng, X. Xu, E. Dubuisson, Q. Bao, J. Lu, and K. P. Loh, *ACS Nano* **5**, 9927 (2011).
59. L. Gao, W. Ren, H. Xu, L. Jin, Z. Wang, T. Ma, L. P. Ma, Z. Zhang, Q. Fu, L. M. Peng, X. Bao, and H.-M. Cheng, *Nat. Commun.* **3**, 699 (2012).
60. H. Li, J. Wu, X. Huang, Z. Yin, J. Liu, and H. Zhang, *ACS Nano* **8**, 6563 (2014).
61. X. Wan, K. Chen, and J. Xu, *Small* **10**, 4443 (2014).
62. C. J. L. de la Rosa, J. Sun, N. Lindvall, M. T. Cole, Y. Nam, M. Lööffler, E. Olsson, K. B. K. Teo, and A. Yurgens, *Appl. Phys. Lett.* **102**, 022101 (2013).
63. I. Jo, M. T. Pettes, J. Kim, K. Watanabe, T. Taniguchi, Z. Yao, and L. Shi, *Nano Lett.* **13**, 550 (2013).
64. S. J. Kang, G. H. Lee, Y. J. Yu, Y. Zhao, B. Kim, K. Watanabe, T. Taniguchi, J. Hone, P. Kim, and C. Nuckolls, *Adv. Funct. Mater.* **24**, 5157 (2014).
65. M. S. Bresnahan, M. J. Hollander, M. Wetherington, M. LaBella, K. A. Trumbull, R. Cavalero, D. W. Snyder, and J. A. Robinson, *ACS Nano* **6**, 5234 (2012).
66. B. Hunt, J. D. Sanchez-Yamagishi, A. F. Young, M. Yankowitz, B. J. LeRoy, K. Watanabe, T. Taniguchi, P. Moon, M. Koshino, P. Jarillo-Herrero, and R. C. Ashoori, *Science* **340**, 1427 (2013).
67. A. S. Mayorov, R. V. Gorbachev, S. V. Morozov, L. Britnell, R. Jalil, L. A. Ponomarenko, P. Blake, K. S. Novoselov, K. Watanabe, T. Taniguchi, and A. K. Geim, *Nano Lett.* **11**, 2396 (2011).
68. H. Wang, T. Taychatanapat, A. Hsu, K. Watanabe, T. Taniguchi, P. Jarillo-Herrero, and T. Palacios, *IEEE Electr. Dev. Lett.* **32**, 1209 (2011).
69. L. A. Ponomarenko, A. K. Geim, A. A. Zhukov, R. Jalil, S. V. Morozov, K. S. Novoselov, I. V. Grigorieva, E. H. Hill, V. V. Cheianov, V. I. Fal'ko, K. Watanabe, T. Taniguchi, and R. V. Gorbachev, *Nat. Phys.* **7**, 958 (2011).
70. L. Britnell, R. V. Gorbachev, R. Jalil, B. D. Belle, F. Scheiden, A. Mishchenko, T. Georgiou, M. I. Katsnelson, L. Eaves, S. V. Morozov, N. M. R. Peres, J. Leist, A. K. Geim, K. S. Novoselov, and L. A. Ponomarenko, *Science* **335**, 947 (2012).
71. M. Yankowitz, J. Xue, D. Cormode, J. D. Sanchez-Yamagishi, K. Watanabe, T. Taniguchi, P. Jarillo-Herrero, P. Jacquod, and B. J. LeRoy, *Nat. Phys.* **8**, 382 (2012).
72. S. J. Haigh, A. Gholinia, R. Jalil, S. Romani, L. Britnell, D. C. Elias, K. S. Novoselov, L. A. Ponomarenko, A. K. Geim, and R. Gorbachev, *Nat. Mater.* **11**, 764 (2012).
73. Z. Liu, L. Song, S. Zhao, J. Huang, L. Ma, J. Zhang, J. Lou, and P. M. Ajayan, *Nano Lett.* **11**, 2032 (2011).
74. M. Wang, S. K. Jang, W.-J. Jang, M. Kim, S.-Y. Park, S.-W. Kim, S.-J. Kahng, J.-Y. Choi, R. S. Ruoff, Y. J. Song, and S. Lee, *Adv. Mater.* **25**, 2746 (2013).
75. J. M. Garcia, U. Wurstbauer, A. Levy, L. N. Pfeiffer, A. Pinczuk, A. S. Plaute, L. Wang, C. R. Deang, R. Buizzaf, A. M. Van Der Zande, J. Hone, K. Watanabe, and T. Taniguchi, *Solid State Commun.* **152**, 975 (2012).
76. T. Gao, X. J. Song, H. W. Du, Y. F. Nie, Y. B. Chen, Q. Q. Ji, J. Y. Sun, Y. L. Yang, Y. F. Zhang, and Z. F. Liu, *Nature Commun.* **6**, 6835 (2015).
77. S. Sharma, G. Kalita, R. Vishwakarma, Z. Zulkifli, and M. Tanemura, *Sci. Rep.* **5**, 10426 (2015).
78. L. Ci, L. Song, C. Jin, D. Jariwala, D. Wu, Y. Li, A. Srivastava, Z. F. Wang, K. Storr, L. Balicas, F. Liu, and P. M. Ajayan, *Nat. Mater.* **9**, 430 (2010).
79. Y.-M. Lin, C. Dimitrakopoulos, K. A. Jenkins, D. B. Farmer, H.-Y. Chiu, A. Grill, and P. Avouris, *Science* **327**, 662 (2010).
80. L. Liao, Y. C. Lin, M. Bao, R. Cheng, J. Bai, Y. Liu, Y. Qu, K. L. Wang, Y. Hunag, and X. Duan, *Nature* **467**, 305 (2010).
81. T. Ando, *J. Phys. Soc. Jpn.* **75**, 074716 (2006).
82. M. Ishigami, J. H. Chen, W. G. Cullen, M. S. Fuhrer, and E. D. Williams, *Nano Lett.* **7**, 1643 (2007).

83. S. V. Morozov, K. S. Novoselov, M. I. Katsnelson, F. Schedin, D. C. Elias, J. A. Jaszczak, and A. K. Geim, *Phys. Rev. Lett.* **100**, 016602 (2008).
84. S. Fratini and F. Guinea, *Phys. Rev. B* **77**, 195415 (2008).
85. J. H. Chen, C. Jang, S. Xiao, M. Ishigami, and M. S. Fuhrer, *Nature Nanotech.* **3**, 206 (2008).
86. R. Decker, Y. Wang, V. W. Brar, W. Regan, H.-Z. Tsai, Q. Wu, W. Gannett, A. Zettl, and M. F. Crommie, *Nano Lett.* **11**, 2291 (2011).
87. J. Xue, J. Sanchez-Yamagishi, D. Bulmash, P. Jacquod, A. Deshpande, K. Watanabe, T. Taniguchi, P. Jarillo-Herrero, and B. J. LeRoy, *Nat. Mater.* **10**, 282 (2011).
88. I. Meric, C. Dean, A. Young, J. Hone, P. Kim, and K. L. Shepard. IEDM Tech. Dig. pp.23.2.1-4 IEEE, San Francisco (2010).
89. C. Berger, Z. Song, Xuebin Li, X. Wu, N. Brown, C. Naud, D. Mayou, T. Li, J. Hass, A. N. Marchenkov, E. H. Conrad, P. N. First, and W. A. de Heer, *Science* **312**, 1191 (2006).
90. L. Britnell, R. V. Gorbachev, R. Jalil, B. D. Belle, F. Schedin, M. I. Katsnelson, L. Eaves, V. Morozov, A. S. Mayorov, N. M. R. Peres, A. H. Castro Neto, J. Leist, A. K. Geim, L. A. Ponomarenko, and K. S. Novoselov, *Nano Lett.* **12**, 1707 (2012).
91. G. H. Lee, Y. J. Yu, C. Lee, C. Dean, K. L. Shepard, and P. Kim, *Appl. Phys. Lett.* **99**, 243114 (2011).
92. C. Dean, A. F. Young, L. Wang, I. Meric, G.-H. Lee, K. Watanabe, T. Taniguchi, K. Shepard, P. Kim, and J. Hone, *Solid State Commun.* **152**, 1275 (2012).
93. B. D. Briggs, B. Nagabhirava, G. Rao, R. Geer, H. Gao, Y. Xu, and B. Yu, *Appl. Phys. Lett.* **97**, 223102 (2010).
94. T. H. Yu, E. Kim, N. Jain, Y. Xu, R. Geer, and B. Yu, IEDM Tech. Dig. pp.7.5.1-4, IEEE, Washington (2011).
95. Y. Sui and J. Appenzeller, *Nano Lett.* **9**, 2973 (2009).
96. N. Jain, C. A. Durcan, R. Jacobs-Gedrim, Y. Xu, and B. Yu, *Nanotechnology* **24**, 355202 (2013).
97. N. Jain, M. Murphy, R. Jacobs-Gedrim, M. Shanmugam, Y. Fan, S. Eui, and Y. Bin, *IEEE Electr. Dev. Lett.* **35**, 1311 (2014).
98. S. A. Han, K. H. Lee, T. H. Kim, W. Seung, S. K. Lee, S. Choi, B. Kumar, R. Bhatia, H.-J. Shin, W.-J. Lee, S. M. Kim, H. S. Kim, J.-Y. Choi, and S.-W. Kim, *Nano Energy* **12**, 556 (2015).
99. L. M. Arden and S. Li, *Mater. Today* **17**, 163 (2014).
100. S. Z. Butler, S. M. Hollen, L. Cao, Y. Cui, J. A. Gupta, H. R. Gutierrez, T. F. Heinz, S. S. Hong, J. Huang, A. F. Ismach, E. Johnston-Halperin, M. Kuno, V. V. Plashnitsa, R. D. Robinson, R. S. Ruoff, S. Salahuddin, J. Shan, L. Shi, M. G. Spencer, M. Terrones, W. Windl, and J. E. Goldberger, *ACS Nano*. **7**, 2898 (2013).
101. J. H. Seol, I. Jo, A. L. Moore, L. Lindsay, Z. H. Aitken, M. T. Pettes, X. Li, Z. Yao, R. Huang, D. Broido, N. Mingo, R. S. Ruoff, and L. Shi, *Science* **328**, 213 (2010).
102. W. Jang, Z. Chen, W. Bao, C. N. Lau, and C. Dames, *Nano Lett.* **10**, 3909 (2010).
103. B. Qiu and X. L. Ruan, *Appl. Phys. Lett.* **100**, 193101 (2012).
104. M. T. Pettes, I. Jo, Z. Yao, and L. Shi, *Nano Lett.* **11**, 1195 (2011).
105. Z. Yan, G. Liu, J. M. Khan, and A. A. Balandin, *Nat. Commun.* **3**, 827 (2012).
106. J. Bao, Y. Zhang, and S. R. Huang, *J. Basic Sci. Eng.* (In press).
107. S. X. Sun, J. Bao, W. Mu, Y. F. Fu, Y. Zhang, L. L. Ye, and J. Liu, *Electr. Comp. Tech. Conf. (ECTC)* pp. 1658-1663, IEEE, San Diego (2015).